Deep-Sea Research I 75 (2013) 28–38

Contents lists available at SciVerse ScienceDirect

Deep-Sea Research I

journal homepage: www.elsevier.com/locate/dsri

Micro-grazer biomass, composition and distribution across prey resource and dissolved oxygen gradients in the far eastern tropical north Pacific Ocean

M. Brady Olson *,[1], Kendra L. Daly

College of Marine Science, University of South Florida, St. Petersburg, FL 33701, USA

ARTICLE INFO

Article history:
Received 27 February 2012
Received in revised form
26 December 2012
Accepted 4 January 2013
Available online 18 January 2013

Keywords:
Micro-grazers
Ciliates
Dinoflagellates
Oxygen minimum zone
Grazing

ABSTRACT

The ecology of micro-grazers (M_g) was investigated across prey and dissolved oxygen (DO) gradients in the eastern tropical north Pacific Ocean (ETNP) during October–November 2007. Surface (<200 m) chlorophyll *a* (Chl *a*) across *a* $\sim$1700 km north–south transect ranged between the seasonal average of 0.2 μg Chl *a* L^{-1} to 1.8 μg Chl *a* L^{-1} in an extensive Chl *a*-rich patch in the center of the transect. Limiting (<20 μmol kg^{-1} O_2) DO concentrations were encountered as shallow as 24 m. Biomass of M_g in waters above the upper oxycline (UO) ranged between 5.6 μg C L^{-1} and 36.6 μg C L^{-1}, with highest M_g biomass observed in locations with highest Chl *a*. Heterotrophic dinoflagellates contributed most, on average, to M_g biomass (41% to 53%), followed by aloricate spirotrich ciliates (24% to 29%) and heterotrophic nanoflagellates (11% to 33%). Biomass of M_g decreased, on average, over 96% in waters below the UO, but this decrease did not appear to be regulated by DO; M_g biomass more strongly correlated with Chl *a* ($r=0.83$, $P<0.001$) and temperature ($r=0.76$, $P<0.001$) at discrete depths than with DO ($r=0.67$, $P<0.001$). Using a multiple stepwise regression model, Chl *a* alone accounted for 68% M_g biomass variability, whereas Chl *a* and temperature combined accounted for 84%. In two M_g grazing experiments we found that M_g removed 33% and 108% of surface primary production in the upper mixed layer. These estimates of M_g grazing, while limited in scope, fall within estimates from other regions of the equatorial Pacific Ocean, and help reinforce the paradigm that M_g are influential in regulating organic carbon dynamics in the eastern tropical Pacific. A primary finding from this study was that observations of M_g biomass are higher than previously reported for the ETNP. This observation suggests that the region's complex air–sea interactions and the resultant positive influence on primary production and phytoplankton biomass can episodically support high biomass of a diverse M_g community.

1. Introduction

The eastern tropical north Pacific Ocean (ETNP) is an atmospherically and hydrographically complex region, whose dynamic nature is derived from many co-occurring factors that vary in magnitude seasonally and interannually (Fiedler and Talley, 2006 and references therein). Briefly, it is the confluence of two major eastern boundary currents, the California Current and the Humboldt Current, and the north Equatorial Counter Current (Kessler, 2006). It is also the convergence zone for the trade winds (Intertropical Convergence Zone; ITCZ) and concentrated wind jets (Willett et al., 2006) blowing over Mexico and Central America. The considerable distance of the ITCZ from land creates a zone in the far eastern ETNP that has little evaporation and vertical mixing, yet receives strong thermal input. These factors act synergistically to create a particularly strong and shallow thermocline in the ETNP (Fiedler and Talley, 2006). In concert with surface productivity, the weak surface mixing and weak deep water ventilation caused by this strong and shallow thermocline acts, in part, to create an expansive sub-oxic zone (oxygen minimum zone [OMZ]) where dissolved oxygen (DO) falls under 20 μmol kg^{-1} below a depth of 20 m to 40 m in this region (Kamykowski and Zentara, 1990; this study).

Much of the far eastern ETNP is characterized by surface water temperatures consistently >27 °C, and is defined as the eastern Pacific warm pool (Fiedler and Talley, 2006). Within this warm pool, primary production is low and chlorophyll *a* (Chl *a*) standing stock is, on average, $\sim$0.2 μg Chl *a* L^{-1} (Pennington et al., 2006). However, the complex air–sea interaction over this otherwise oligotrophic region episodically promotes high phytoplankton productivity and standing stock biomass (>2.0 μg Chl *a* L^{-1}) through two hydrographic features that vary in magnitude seasonally (Fiedler, 2002; Xie et al., 2005). First, a doming of the thermocline to $\sim$15 m at a mean location of 9°N, 90°W at the

* Corresponding author. Tel.: +1 360 293 2188; fax: +1 360 293 1083.
E-mail address: brady.olson@www.edu (M. Brady Olson).
[1] Present address: Shannon Point Marine Center, Western Washington University, 1900 Shannon Point Road, Anacortes, WA 98221, USA.

0967-0637/$ - see front matter © 2013 Elsevier Ltd. All rights reserved.
http://dx.doi.org/10.1016/j.dsr.2013.01.001

terminus of the west to east shoaling equatorial countercurrent thermocline ridge marks the Costa Rica Dome (Fiedler, 2002). The cyclonic flow around this dome generates Ekman pumping and upwelling that, in turn, promotes elevated phytoplankton productivity (Fiedler, 2002). The strength, location and productivity within the dome vary seasonally through atmospheric forcing associated with the migration of ITCZ and intensification of local winds in the boreal winter (Fiedler and Talley, 2006). Second, winter-time atmospheric pressure over the Gulf of Mexico and the Caribbean is higher than over the Pacific Ocean. As a result, strong winds (wind jets) blow through narrow gaps in the Sierra Madre mountain range and into the ETNP (Xie et al., 2005; Willett et al., 2006). These strong winds initiate upwelling and surface mixing near the coast, and as the winds move offshore, they generate positive wind stress curl which promotes the development of off-shore migrating eddies and Ekman pumping. The enhanced biological productivity associated with these wind jets and eddies can be substantial (Müller-Karger and Fuentes-Yaco, 2000) and introduce high biological variability into the ETNP (Pennington et al., 2006).

Outside of these episodic 'biological hotspots,' phytoplankton production in the ETNP is typically dominated by picophytoplankton (Chavez, 1989) due to the low surface nitrate concentrations resulting from the strong stratification and weak vertical mixing (Yang et al., 2004; Pennington et al., 2006). It is well-established that in systems dominated by small-sized phytoplankton, including the ETNP, micro-grazers (M_g) play a vital role in the trophic transfer and remineralization of organic carbon (Sherr and Sherr, 1994). Consumption of phytoplankton production by M_g can be in excess of 100% in the central (Landry et al., 1995a; Verity et al., 1996) and eastern (Landry et al., 2000, 2011; Yang et al., 2004) equatorial Pacific Ocean. Using published laboratory feeding rates and measured M_g biomass, Beers and Stewart (1971) quantitatively estimated the ecological and grazing impact of M_g in the ETNP. Their estimates, integrated over the euphotic zone, suggest that M_g remove 39% to 104% (average 70%) daily primary production in the ETNP. That study, however, was conducted prior to the recognition of the quantitative and ecological importance of heterotrophic dinoflagellates (Lessard and Swift, 1986; Lessard, 1991); as such, those approximations may potentially underestimate the importance of M_g in the region. Yang et al. (2004) characterized the ecology of M_g across interfaces of surface water divergence and convergence at the westward end of the ETNP, and found that M_g grazing accounted for between 86.8% and 140.3% primary production, and biomass of M_g reached 11.3 $\mu g\ C\ L^{-1}$.

What remains poorly understood in the ETNP is (1) how the M_g community composition and biomass changes across the biological hotspots described above, and (2) to what extent the pronounced and shallow OMZ ($<20\ \mu mol\ kg^{-1}$) in this dynamic region regulates the distribution, abundance and composition of M_g. Mesozooplankton distribution and abundance is, comparatively, highly restricted by the OMZ in the ETNP, with the exception of specialists adapted to low oxygen conditions (reviewed by Fernández-Álamo and Färber-Lorda (2006)). In this study, we quantified the horizontal and vertical distribution, biomass concentration, and composition of the M_g community in the ETNP across resource gradients, and in relation to DO concentration. We also measured grazing and net growth rates of the M_g community in upper mixed layer depths in two experiments at locations contrasting in hydrography and averaged seasonal productivity (Pennington et al., 2006): the unproductive eastern Pacific warm pool (Fiedler and Talley, 2006) and the mean location of the Costa Rica Dome.

2. Materials and methods

2.1. Study site, environmental conditions and chlorophyll a

During a fall cruise (18 Oct.–17 Nov. 2007) in the ETNP we conducted a series of analyses to determine the distribution, abundance, and grazing impact of M_g in this biologically and hydrographically diverse region. Eight stations (Sta.) were sampled along a 1700 km transect, which began in the core of the eastern Pacific warm pool, and crossed over to the presumptive core of the productive Costa Rica Dome (Fig. 1). *In situ* environmental parameters at the time and depth of experimental water collection were recorded using a conductivity, temperature, pressure (CTD) profiling system (Sea-Bird 3*plus* temperature sensor, Sea-Bird 9*plus* digital quartz pressure sensor, Seabird 4C conductivity sensory) equipped with a Seabird 43 oxygen sensor and a C-Point chlorophyll fluorescence sensor. Seawater for biological and chemical analysis, as well as for experiments, was collected using a rosette of 24 10-L Niskin bottles. Analysis of these samples is described in Section 2.4.

2.2. Micro-grazer distribution and abundance

Discrete samples from multiple depths were taken at stations for estimates of M_g biomass concentration, distribution, and composition. Here we describe M_g as zooplankton encompassing a size range between 2 μm and 200 μm in length, including heterotrophic nanoflagellates (HNF), ciliates, heterotrophic dinoflagellates, and because they occupy the same trophic position, we include metazoans <200 μm in length.

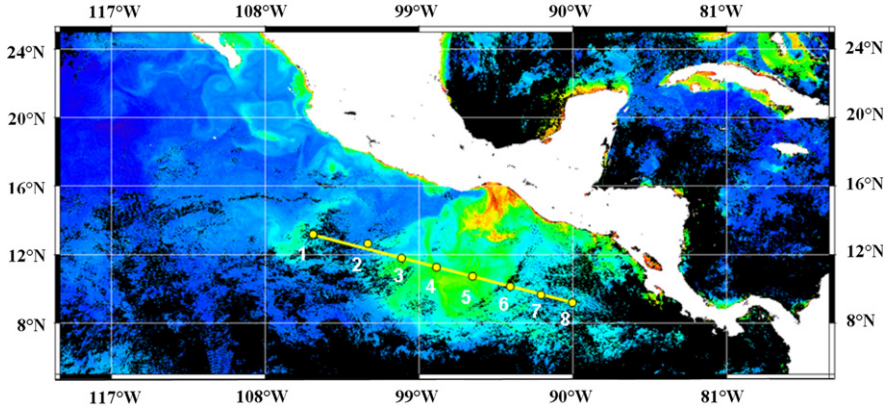

Fig. 1. Aqua MODIS (Moderate Resolution Imaging Spectroradiometer) level 3 data showing Oct. 2007 monthly mean (9 km resolution) surface chlorophyll at our study site. Station locations are denoted by number. See Table 1 for station latitude and longitude.

To determine what environmental and biological variables influence M_g community composition, vertical distribution and biomass concentration, discrete sampling depths were chosen based on chemical and biological signatures, rather than arbitrary, yet consistent, depths. Our defined biological and chemical sampling regimes across all stations were surface waters, the pigment maximum (determined from CTD fluorescence), and, because a defining feature of this region is the vast extent of the OMZ, both vertically and horizontally, we sampled the upper oxycline (UO; the depth near surface where the decrease in DO concentration is greatest), the middle of the OMZ, and the lower oxycline (LO; depth below OMZ where DO concentrations increase). The depths of the biological and chemical features were determined from vertical profiles using the Sea-Bird Electronics 911*plus* CTD profiler described above. For each discrete location and depth, duplicate samples of 200 ml were taken for M_g analysis (described in Section 2.4).

2.3. Micro-grazer grazing experiments

Two M_g grazing experiments were conducted to preliminarily explore the degree to which grazing regulates the accumulation of phytoplankton production in two contrasting regions in the ETNP (Sta. 1, core of the eastern Pacific warm pool, and Sta. 8, mean position of the Costa Rica Dome). Specific growth rate (μ, d^{-1}) and specific M_g grazing rate (g, d^{-1}) for the aggregate Chl *a* community were estimated simultaneously using the seawater dilution technique (e.g., Landry et al., 1995b). Seawater was collected in 10 L Niskin bottles from depths in the upper-mixed layer corresponding to 50% surface PAR. Particle-free diluent water was made by gently draining the entire contents of two 10 L Niskin bottles through silicone tubing into a 20 L polycarbonate carboy. This pooled water was then gravity-filtered through a 0.2 μm Pall Gelman pleated capsule filter into a second 20 L carboy. Whole seawater for our dilution experiments was collected from the same CTD cast as diluent water. Whole seawater was very gently drained through silicone tubing encased with 200 μm mesh to remove abundant mesozooplankton and dispensed into a 20 L carboy.

Measured volumes of particle-free seawater were transferred into a series of 1.125 L polycarbonate bottles. Whole seawater was gently siphoned from the whole seawater carboy into the bottles containing particle-free water. Although large, rapidly-sinking phytoplankton were seemingly rare, the whole seawater was kept well-mixed by very gentle stirring with a polyethylene plunger. Combinations of particle-free to whole seawater were made to achieve target dilutions in duplicate of 20%, 40%, 60%, 80% and 100% whole seawater. Experimental bottles were amended with nutrients (5 μM NH_4^+ and 0.31 μM PO_4^{3-}) in order to remove potential bias from enhanced phytoplankton growth rate due to variable M_g nutrient excretion across dilution treatments. An additional set of 100% whole seawater bottles were incubated without nutrient-addition to correct for this potential bias (see below). Quadruplicate samples of whole seawater were taken at random intervals from the whole seawater carboy during experimental set-up for analysis of initial Chl *a* (100 ml to 500 ml), and duplicate samples were drawn for analysis of inorganic nutrient concentration (~20 ml) and M_g abundance and biomass (200 ml each).

Experimental dilution bottles were screened with a single layer of neutral density screening to mimic in situ light levels at the depth of collection (50% surface PAR). Bottles were then placed in on-deck incubators supplied with continuous flow of surface seawater and allowed to incubate for 24 h. After incubation, each replicate dilution bottle was sampled in duplicate for Chl *a*. Samples were taken from the two 100% whole seawater bottles for analysis of final M_g composition and biomass.

Net growth rate (k, d^{-1}) of the aggregate Chl *a* community in each replicate dilution bottle was determined in duplicate as $(1/t)(\ln[P_t/P_o])$, where P_t and P_o are the final and initial Chl *a* concentrations, respectively, and t is the duration of the incubation in days. Initial Chl *a* concentrations from dilution bottles were calculated by multiplying the initial concentration of Chl *a* in the 100% whole seawater by dilution level. Regression of the Chl *a* net growth rates across each respective whole seawater dilution factor yields the intrinsic growth rate (μ, d^{-1}) of the Chl *a* community as the ordinal intercept. The negative slope of the regression yields the M_g community grazing rate (g, d^{-1}). When nutrient-limited growth was observed in unamended 100% whole seawater controls, corrections to μ were made to yield unamended intrinsic growth rates according to $\mu_{un}=k_{un\ 100\%\ WSW}+g$, where $k_{un\ 100\%\ WSW}$ is the net growth rate in the 100% whole seawater treatment without added nutrients.

Net growth rates of specific M_g functional groups (kM_g, d^{-1}) were calculated using biomass estimates made from cell counts. Estimates of kM_g were calculated using $(1/t)(\ln[M_{gt}/M_{go}])$, where M_{gt} and M_{go} are the biomass of the respective M_g groups in the 100% whole seawater final bottles and initial whole seawater, respectively.

2.4. Sample preservation and analysis

Samples taken for Chl *a* analysis from transect stations, and for dilution experiments, the whole seawater carboy and final dilution bottles (between 100 ml and 500 ml), were filtered onto Whatman GF/F filters within 20 min of collection at <7 mm Hg vacuum pressure. Filters were immediately placed in 13 mm borosilicate test tubes containing 90% v/v HPLC grade acetone and extracted in darkness for 24 h at -20 °C. After extraction, fluorescence was measured with a Turner Designs 10AU fluorometer and Chl *a* determined using the methods of Parsons et al. (1984). The fluorometer was calibrated at sea using pure Chl *a* standards (Turner Designs).

As mentioned, 200 ml samples were taken from discrete depths at different stations, from the whole seawater carboy during experimental set-up, and from final dilution bottles for two types of M_g preservation and analysis. Immediately after collection, one 200 ml sample was preserved in 5% final concentration Lugol's acid for analysis of large heterotrophic dinoflagellates, ciliates, and mesozooplankton <200 μm in length. The other 200 ml sample was immediately preserved in 0.5% final concentration buffered glutaraldehyde for analysis of HNF, small (<20 μm) heterotrophic dinoflagellates, and sarcodines. The glutaraldehyde-fixed samples were stained with 4′6-diamidino-2-phenylindole (DAPI) and proflavin, filtered onto 0.2 μm and 0.8 μm black polycarbonate filters, and slide-mounted on slides using Resolve® microscope immersion oil. Slides were stored in darkness at -20 °C until analysis.

Upon returning to the laboratory, 50 ml from each Lugol's-fixed sample was allowed to settle for 24 h in graduated cylinders, after which the top 40 ml was decanted off and the remaining 10 ml resettled into Utermöhl chambers for an additional 24 h. Large heterotrophic dinoflagellates, ciliates, and small mesozooplankton were counted and measured using an Olympus inverted microscope at X400. HNF, small heterotrophic dinoflagellates (<20 μm), and sarcodines were counted and measured on the glutaraldehyde-fixed slides using an Olympus epifluorescent microscope. Cell measurements were made by interfacing each microscope with a computer-aided digitizing system (Roff and Hopcroft, 1986). Linear measurements of individual M_g were used to calculate cell biovolume, which was, in turn, used to calculate cell biomass using the general protist equation from Menden-Deuer and Lessard (2000).

Initial nutrient concentrations from our grazing experiments were determined by collecting ~20 ml samples from the whole seawater carboy. Samples were frozen at −20 °C and analyzed on shore using a Technicon Autoanalyzer II using the methods of Gordon et al. (1993).

2.5. Statistical analysis

All statistical analyses were made using IBM SPSS 20 software. Correlations between variables were determined using a Pearson Product Moment Correlation, and are reported as Pearson's *r*. Examination of M_g biomass data using the Shapiro–Wilk test revealed that the data were non-normally distributed ($P < 0.05$). As such, to meet the assumption of normality, the M_g biomass data were square root transformed in all analyses. A multiple stepwise regression analysis was performed to determine which factor or combination of factors (Chl *a*, DO, temperature, salinity) best described the variability in M_g biomass. For this model we used probability criteria, such that for any sequence or combination of factors, factor entry into the model required $P \leq 0.05$, and removal from the model occurred when $P \geq 0.1$. In stepwise regression, at each step of the model all eligible variables are considered for removal or entry. Multicollinearity of predictor variables included in our model was determined using the variance inflation factor (VIF). We determined a priori that VIF values >10 would disproportionately influence our model. The linear regression assumptions of linearity, independence, homoscedasticity and normality were satisfied prior to running the model. Linearity and homoscedasticity were assessed and both were determined satisfactory by plotting residuals against all sets of independent variables and observing constant variance along a horizontal line.

3. Results

3.1. Hydrography and chlorophyll a

Surface water temperatures were highest at the northern (28 °C) and southern Stas. (> 27 °C). Lowest surface temperatures (25.5 °C) and doming of isotherms were found at the mid Stas. (Table 1; Fig. 2). With the exception of Sta. 2 (32.5 psu), surface salinity was between 33.0 and 33.7 at all other Stas. (Table 1). Surface DO at all stations was between 174 μmol kg^{-1} and 218 μmol kg^{-1} and the depth of the UO varied between 24 m and 60 m across stations (Figs. 2 and 3). A pronounced doming of DO isobars was observed at mid Stas. (Fig. 2). Concentrations of DO in the OMZ were below 20 μmol kg^{-1} at all locations (Fig. 2).

Lowest Chl *a* concentration was observed at Sta. 1 (0.4 μg Chl *a* L^{-1}), and began to increase towards mid stations (Fig. 2). An extensive region of comparatively high Chl *a* concentration was observed between Stas. 3–6 (Figs. 1 and 2), with the highest measured concentration (> 1.8 μg Chl *a* L^{-1}) found at 10 m depth at Sta. 5. Chlorophyll *a* was consistently found in excess of 0.8 μg Chl *a* L^{-1} above 50 m at Stas. 3–6. Chlorophyll *a* concentration was again low at Sta. 7, reaching only 0.4 μg Chl *a* L^{-1} at 40 m depth. Chlorophyll *a* concentration began to rise again at Sta. 8, with concentrations approaching 0.8 μg Chl *a* L^{-1} beginning at 20 m depth (Fig. 2).

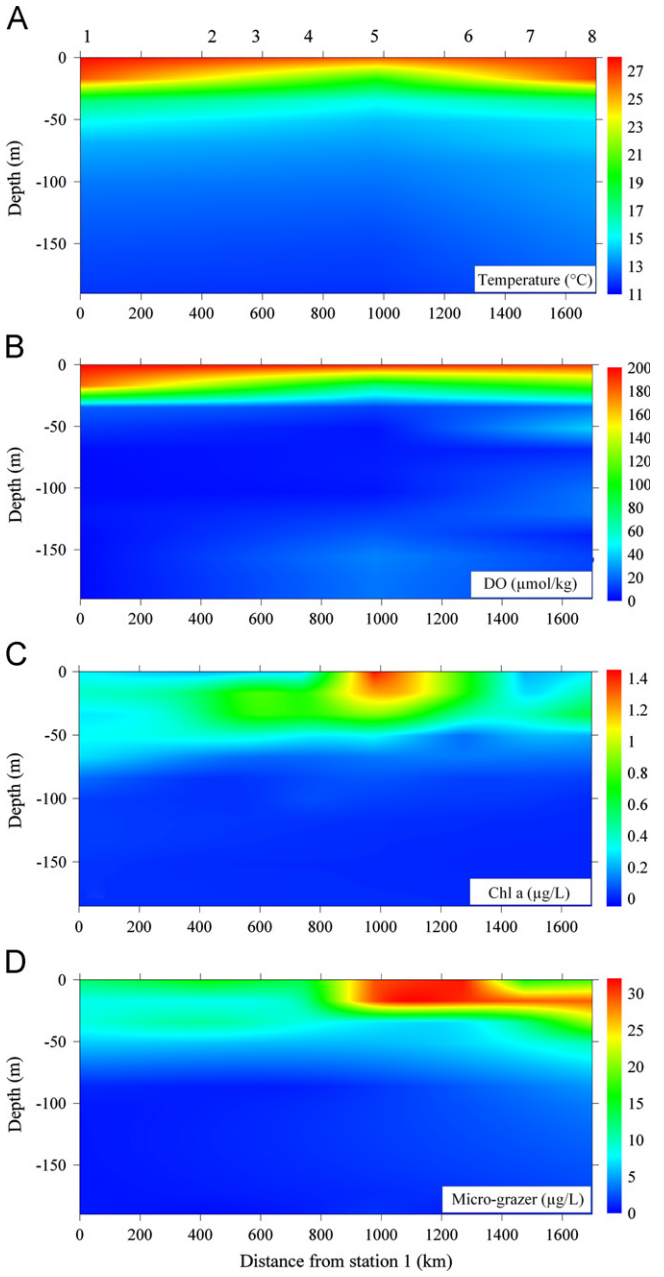

Fig. 2. North to south surface sections (< 200 m) showing (A) temperature, (B) DO, (C) Chl *a* and (D) M_g biomass. Station locations are shown above panel A. Distance from Sta. 1 is denoted on the *x*-axis. Temperature and DO were measured using Sea-bird 3*plus* temperature sensor and a Sea-bird 43 oxygen sensor. Seawater was collected at each station location using CTD for determination of Chl *a* and M_g biomass.

Table 1
Sampling and experimental station location and surface characteristics. N: north; W: west; n.d.: no data available.

Station	Latitude (N)	Longitude (W)	Surface temp (°C)	Salinity (psu)	Surface Chl *a* (μg Chl *a* L^{-1})
1	13° 00.06	105° 00.04	28.0	33.4	0.31
2	11° 59.97	101° 13.69	28.1	32.5	0.21
3	11° 37.44	99° 50.50	28.1	33.0	n.d.
4	11° 14.56	98° 24.63	26.7	33.7	0.26
5	10° 41.36	96° 20.47	25.5	33.3	1.43
6	9° 59.92	93° 43.46	26.9	33.4	0.77
7	9° 31.29	91° 57.11	27.3	33.5	0.21
8	9° 00.03	89° 59.99	27.1	33.4	0.21

3.2. Micro-grazer biomass, distribution and composition

Maximum biomass concentrations of M_g ranged from 5.6 μg C L^{-1} to 36.6 μg C L^{-1} in waters above the UO (Table 2; Figs. 2 and 3).

In general, M_g biomass increased between the northern (Sta. 1) and southern stations (Sta. 8; Fig. 2), with the highest M_g biomass observed near the Chl *a* maximum found at Sta. 5 (Table 2; Figs. 2 and 3). Typically, M_g biomass maxima were highest in surface waters, except at Stas. 5 and 8, where highest M_g biomass concentrations were found at the depth of the pigment maximum (25–30 m) (Fig. 3; Table 2). In addition, Sta. 8 had a secondary biomass maximum in the UO at 35 m (Fig. 3). Total M_g biomass decreased below the UO, with values below this depth ranging from 0.2 μg C L^{-1} to 2.9 μg C L^{-1} (Table 2). The highest biomass that we observed below the UO (2.9 μg C L^{-1}) was within the OMZ at Sta. 8, where the community assemblage consisted mostly of HNF and small heterotrophic dinoflagellates.

When depth regimes across stations were averaged, heterotrophic dinoflagellates dominated biomass (> 40% in all cases) (Fig. 4). Within the heterotrophic dinoflagellate functional group, small (< 20 μm) heterotrophic gymnodinoids predominated, contributing between 26% and 43% of the total dinoflagellate biomass. Large, diatom-consuming *Gyrodinium* spp. dinoflagellates were also relatively abundant (Table 2). On rare occasions, other dinoflagellates contributed to total M_g biomass. For example, at Sta. 5 we observed diatom-consuming Protoperidinoid dinoflagellates, which contributed 6.4% to total M_g biomass. The chloroplast-containing dinoflagellates, *Torodinium teredo* and *Brachydinium capitatum*, were also present in most samples from the upper depths, but they contributed very little to total dinoflagellate biomass.

Spirotrich ciliates, including tintinnids, generally contributed less to total M_g biomass than dinoflagellates, but were abundant at all stations and at all depths above the UO, averaging between 24% and 29% of M_g biomass (Table 2; Fig. 4). Below the UO, ciliate contribution to total M_g biomass declined to ~15%. At two Stas. (5 and 6) ciliate biomass was greater than dinoflagellate biomass in surface waters (Fig. 2). At Sta. 6, a 'bloom' of the mixotrophic ciliate *Myrionecta rubra* was observed (16.4 μg C L^{-1}), contributing 88% to ciliate biomass and 52% to total M_g biomass. Tintinnid ciliates were observed at most Stas. in low biomass, with the exception of Stas. 5 and 8 (Table 2), where they contributed moderately to total ciliate biomass, at 2.8% and 3.7%, respectively. Holotrich ciliates were present at all Stas., and their biomass appeared to increase in the vicinity of the UO and in the OMZ (Table 2). Although total ciliate biomass was low in these locations relative to surface waters, holotrich ciliates contributed as much as 87% percent to total ciliate biomass in these oxygen-deprived environments (e.g., Sta. 2, OMZ).

The biomass of HNF in waters above the UO ranged from 0.5 μg C L^{-1} to 10.8 μg C L^{-1} (Table 2). The highest HNF biomass was observed at Sta. 5 in the upper 20 m (Fig. 3). The relative contribution of HNF to total M_g biomass showed an inverse trend to that of ciliates (Fig. 4); the percent contribution of these small protists declined with depth between the surface and UO, but then increased in relative contribution to total biomass in the OMZ and LO (Fig. 4).

Sarcodines (including radiolarians, foraminiferans, and acantharians) were found at most depths in the upper water column (Table 2). On average, sarcodines contributed < 10% to the total biomass (Fig. 4); however, in less-productive waters (Stas. 1 and 4), sarcodines contributed nearly 20% to total M_g biomass at some depths (Table 2). Nauplii of copepods were also observed in surface or pigment maximum depths and, due to their comparatively large size, often were a substantial component of total M_g biomass (Table 2). Nauplii biomass followed the same general trend as did M_g, whereby highest biomass (> 3 μg C L^{-1}) was found at the central and southern stations. Except for one station (Sta. 5), nauplii were not observed below the UO (Table 2).

Total M_g biomass was positively correlated with Chl *a* biomass (Fig. 5) at discrete depths (r=0.83, P < 0.001) and integrated above the UO (r=0.88, P < 0.01). Total M_g biomass was also positively correlated with temperature (r=0.76, P < 0.001) and DO (r=0.67, P < 0.001), although to a lesser extent. Using a multiple stepwise regression analysis of Chl *a*, DO, temperature

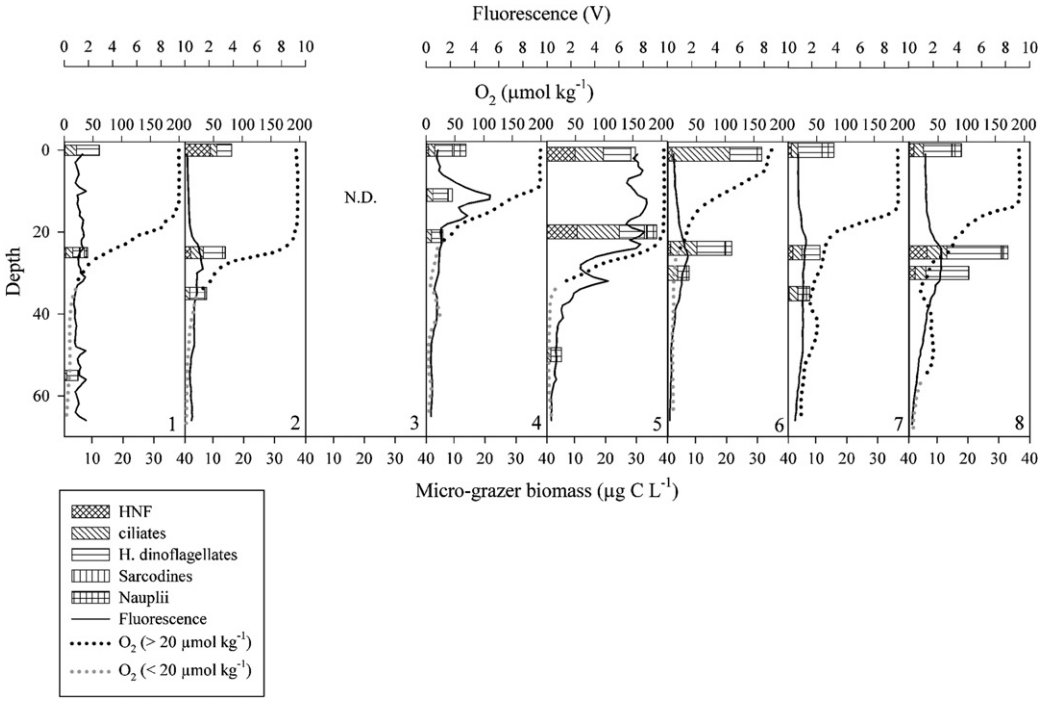

Fig. 3. Vertical profiles of the different sampling sites (numbered at lower right of each panel) showing M_g biomass distributions at surface, pigment maximum, and UO depths in relation to DO concentrations (dotted line) and fluorescence (solid line) in the upper 60 m. Data are not available for Sta. 3. HNF: heterotrophic nanoflagellates; H: heterotrophic.

Table 2
Micro-grazer functional group biomass across the ETNP. Biomass is expressed as μg C L^{-1}. Depths are expressed as both meters and the biochemical regime (see Section 2.2). S: surface; PM: pigment maximum; UO: upper oxycline; OMZ: oxygen minimum zone; LO: lower oxycline: HNF: heterotrophic nanoflagellates; Tint: tintinnid ciliates; Holo: holotrich ciliates; Gymno: *Gymnodinium*-like; Gyro: *Gyrodinium*-like; Sarco: Sarcodines; ND: no data.

Station/depths	HNF	Micro-grazer biomass (μg C L^{-1})										
		Ciliates					Heterotrophic dinoflagellates					
		Spirotrichs										
		< 20 μm	20–40 μm	> 40 μm	Tint.	Holo.	Gymno.	Gyro.	Other	Sarco.	Nauplii	Total
1												
S	1.3	0.5	1.1	1.9	0.1	0.1	2.1	5.1	0.1	–	0.2	12.4
PM-30 m	1.6	0.3	0.5	1.1	–	0.2	0.8	1.3	< 0.1	1.5	1.1	8.6
UO-60 m	0.6	0.2	0.7	0.2	–	0.3	1.0	2.5	< 0.1	0.2	–	5.6
OMZ-200 m	0.5	< 0.1	–	–	–	–	0.1	0.2	< 0.1	–	–	0.8
LO-1100 m	0.2	–	–	–	–	–	0.1	–	–	–	–	0.3
2												
S	9.2	0.4	1.0	0.7	–	–	3.1	1.1	0.6	–	–	16.1
PM-30 m	2.8	0.3	1.3	2.7	–	–	3.0	2.5	0.7	–	0.9	14.0
UO-40 m	0.7	0.6	0.9	0.5	0.1	–	2.5	2.2	< 0.1	0.4	0.4	8.1
OMZ-500 m	0.1	–	< 0.1	–	–	0.1	0.1	< 0.1	–	–	–	0.4
LO-1000 m	< 0.1	–	–	–	–	–	0.1	–	–	–	–	0.2
3												
ND												
4												
S	1.7	0.4	0.5	1.2	< 0.1	–	4.2	1.4	–	0.6	3.9	13.8
PM-18 m	1.2	0.5	0.6	0.8	< 0.1	0.1	3.7	1.0	< 0.1	1.5	–	9.4
UO-24 m	0.7	0.7	0.4	0.8	–	< 0.1	2.5	0.8	0.1	< 0.1	0.5	6.5
OMZ-80 m	0.2	< 0.1	0.1	–	–	< 0.1	0.4	0.1	–	–	–	0.8
LO-200 m	0.2	< 0.1	0.1	0.2	–	< 0.1	0.6	< 0.1	< 0.1	–	–	1.3
5												
S	10.2	1.4	2.6	5.0	< 0.1	–	3.6	3.5	1.9	1.3	–	29.6
PM-20 m	10.8	1.7	1.7	9.8	0.4	–	5.1	2.9	0.1	0.7	3.4	36.6
UO-50 m	0.5	0.4	0.4	1.1	< 0.1	–	2.2	1.2	< 0.1	0.1	–	5.8
OMZ-200 m	0.2	< 0.1	–	–	< 0.1	0.1	0.4	0.7	< 0.1	–	0.2	1.5
LO-1000 m	0.1	–	< 0.1	–	–	–	0.1	< 0.1	–	–	–	0.3
6												
S	2.4	0.3	16.4	2.1	–	–	4.9	3.9	0.1	–	1.5	31.4
UO-24 m	2.0	1.9	2.4	4.0	–	0.1	6.8	2.1	0.1	–	2.3	21.7
PM-30 m	0.8	0.8	1.7	0.6	0.1	0.1	1.7	1.2	–	0.1	0.7	7.9
OMZ-200 m	0.3	< 0.1	< 0.1	–	–	< 0.1	0.4	< 0.1	–	< 0.1	–	0.7
LO-ND												
7												
S	2.1	0.7	0.8	0.5	< 0.1	–	7.1	0.6	0.2	–	3.9	15.8
PM-30 m	2.7	0.8	1.8	0.3	–	–	4.2	1.6	< 0.1	< 0.1	–	11.3
UO-40 m	1.4	0.9	1.5	0.4	–	–	2.3	0.6	–	–	1.0	8.0
OMZ-200 m	0.3	0.1	0.1	–	–	–	0.6	< 0.1	–	–	–	1.2
LO-ND												
8												
S	2.6	0.6	1.0	1.3	< 0.1	0.1	7.9	1.4	< 0.1	0.1	3.1	18.0
PM-30 m	6.8	2.1	3.6	0.5	0.2	–	14.3	3.1	0.1	0.5	1.8	32.9
UO-35 m	3.0	1.0	2.2	0.1	0.1	0.1	12.4	1.4	–	0.1	–	20.4
OMZ-355 m	0.2	0.1	< 0.1	0.6	–	0.3	0.7	0.9	–	0.2	–	2.9
LO-1200 m	0.1	< 0.1	0.1	–	–	–	0.1	0.2	–	–	–	0.5

and salinity against M_g biomass from all depths at all locations, Chl *a* concentration alone accounted for 68% of the M_g biomass variability. Chl *a* concentration combined with temperature was the best predictor of M_g biomass, accounting for 83% of M_g variability.

3.3. Micro-grazer grazing

The environmental conditions found at the M_g grazing experiment stations varied in some aspects, yet were similar in others (Table 3; Fig. 6). Surface seawater temperature was 1 °C warmer at Sta. 1 than at Sta. 8, while surface Chl *a* concentrations at both Stas. were ~0.2 μg Chl *a* L^{-1} (Table 3), despite observed seasonal differences in productivity (Pennington et al., 2006). Inorganic macronutrient concentrations were higher at Sta. 8 compared to those found at Sta. 1 (Table 3). The pigment maximum occurred near the base of the UO at both stations (Fig. 6). At Sta. 1, there was a second deeper pigment maximum (ca. 60–70 m) associated with a sub-surface accumulation of *Rhizosolenia* spp. diatoms. In addition, the depth of the UO was shallower (~20 m) at Sta. 8.

Although the phytoplankton community growth rate was on average higher at Sta. 1 (0.72 d^{-1}) than at Sta. 8 (0.47 d^{-1}), these rate measurements were not statistically different ($P > 0.05$, paired *t*-test). The phytoplankton community at Sta. 1 did, however, show evidence of nutrient limitation. The results from the Sta. 1 experiment showed that the aggregate phytoplankton

community significantly increased their net growth rate ($P < 0.01$, paired t-test) when amended with nutrients (Fig. 7). At Sta. 8 in surface waters, which was centered in the mean core location of the Costa Rica Dome (Fiedler, 2002) where upwelling is thought to occur year-round, inorganic macronutrients were observed at comparatively high concentrations (Table 3) and the phytoplankton community did not show evidence of nutrient-limited growth (Fig. 7; $P > 0.05$, paired t-test).

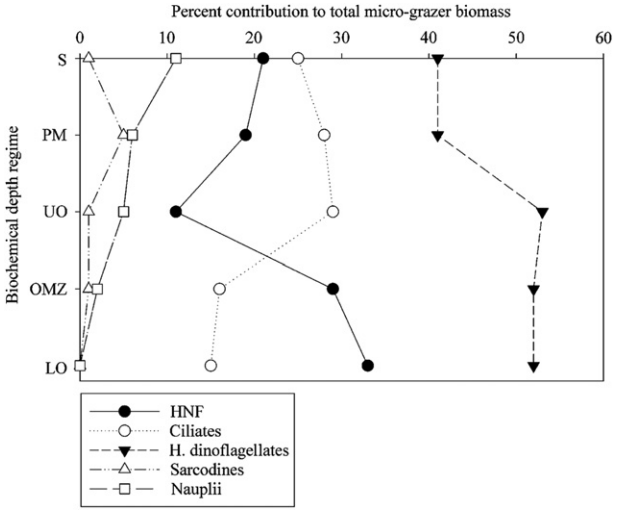

Fig. 4. Percent contribution of different M_g functional groups to the total M_g community biomass. Lines are shown for clarity and are not meant to be interpolations. Each data point represents the averaged biomass for the respective M_g functional groups at each biochemical regime (see Section 2) from each station. HNF: heterotrophic nanoflagellates; H: heterotrophic.

Measured grazing rates by the M_g community were 0.23 d^{-1} and 0.51 d^{-1} at Stas. 1 and 8, respectively (Table 4). Despite the average difference between these two grazing rates, they too were not statistically different ($P > 0.05$, paired t-test). Coupled with the corresponding phytoplankton growth rate, these grazing rates equate to losses of 33% and 108% primary production at Stas. 1 and 8, respectively.

In our dilution experiments M_g biomass (Fig. 8) was similar ($P > 0.05$, paired t-test) between Sta. 1 (12.6 μg C L^{-1}) and Sta. 8 (10.0 μg C L^{-1}). There was, however, an apparent shift in the distribution of M_g functional groups between Sta. 1 and 8 (Fig. 8), whereby the heterotrophic dinoflagellate:ciliate ratio at Sta. 1 was 5.5, compared to 1.8 at Sta. 8. This was a consequence of high gymnodinoid biomass at Sta. 1, and higher ciliate biomass at Sta. 8.

3.4. Micro-grazer growth

Averaged M_g net growth rates measured over the 24 h incubation from our dilution experiments showed a high degree of variance. Despite this, net growth rates were generally low, and for some functional groups, negative (Fig. 9). Low sample size prevented rigorous statistical analysis of these results, but with the high observed variance it is unlikely net growth rates were different from zero for all M_g functional groups.

4. Discussion

4.1. Hydrography and chlorophyll a

Micro-grazers play a significant role in linking microbial and phytoplankton processes to higher trophic levels in all ocean

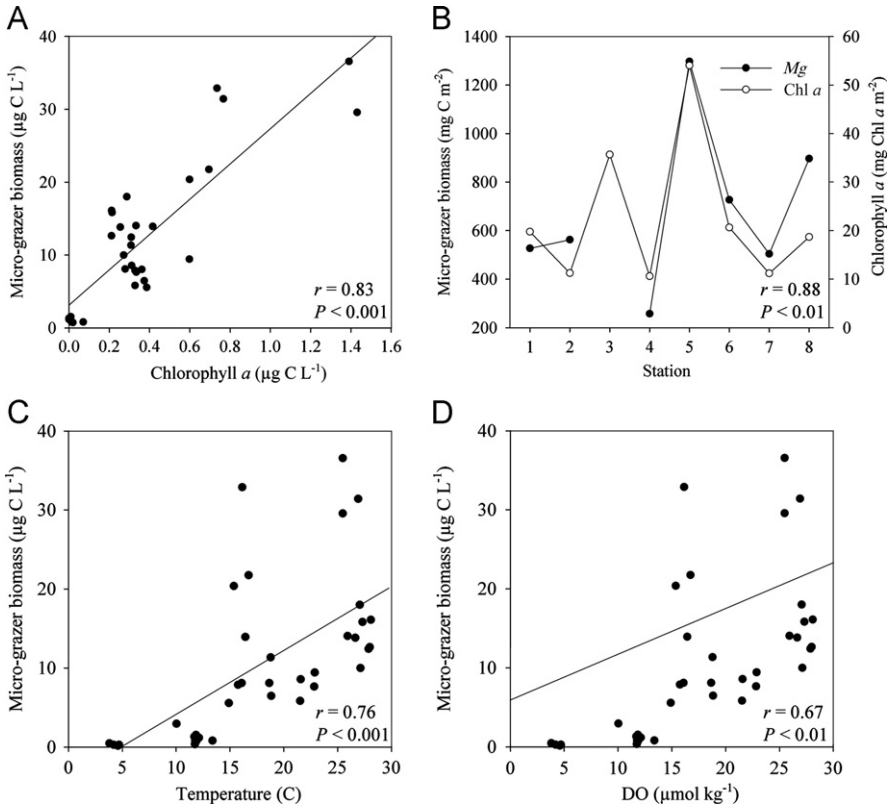

Fig. 5. Correlations between (A) M_g and Chl a biomass from discrete depths ≤ 200 m, (B) M_g and Chl a biomass integrated from depths above the UO, (C) and (D) M_g biomass and temperature and DO, respectively, from depths ≤ 200 m. Pearson's r and P values were determined from square root transformed M_g values. Untransformed data were used in plots.

Table 3
Micro-grazer grazing experiment dates, locations, depth of water collection, surface temperatures, and initial biological and environmental parameters determined from whole seawater during experimental setup. The depths correspond to 50% surface irradiance. Sta: station.

Sta	Date	Latitude (N)	Longitude (W)	Depth (m)	Temp (°C)	Chl *a* (μg L^{-1})	Nutrients (μM)			
							Nitrate	Ammonium	Phosphate	Silicic acid
1	11/01/07	13° 0.94	105° 1.13	9	28.0	0.21 ± 0.02	0.0	0.53	0.26	1.1
8	11/08/07	8° 59.85	90° 0.06	9	27.0	0.27 ± 0.03	5.4	1.08	0.70	3.1

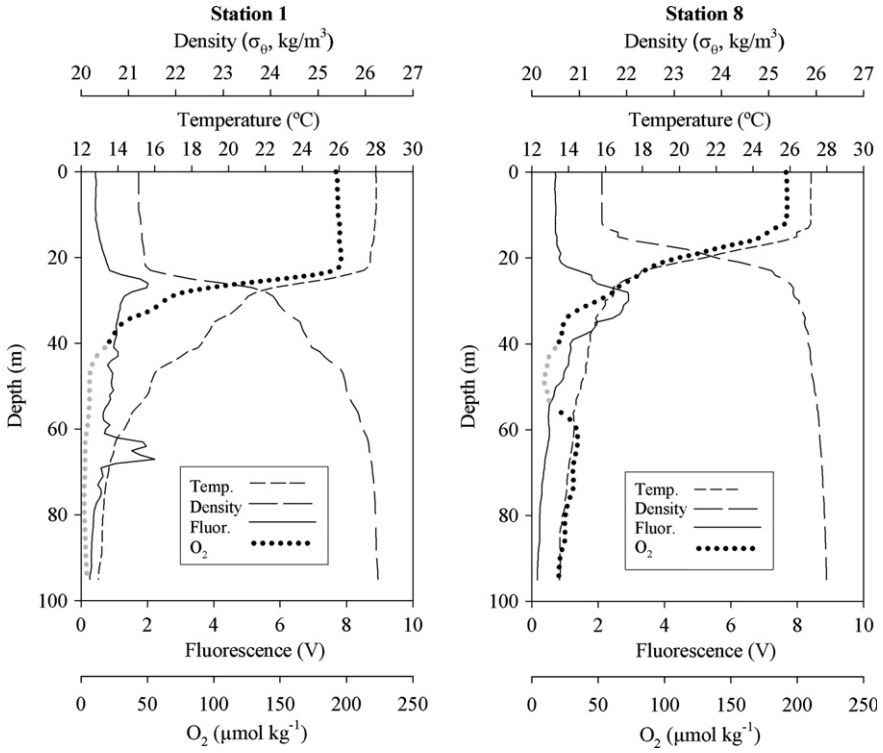

Fig. 6. Hydrographic and biological vertical profiles from M_g grazing experiment stations. Dissolved oxygen concentrations below 20 μmol kg^{-1} are denoted as grey circles.

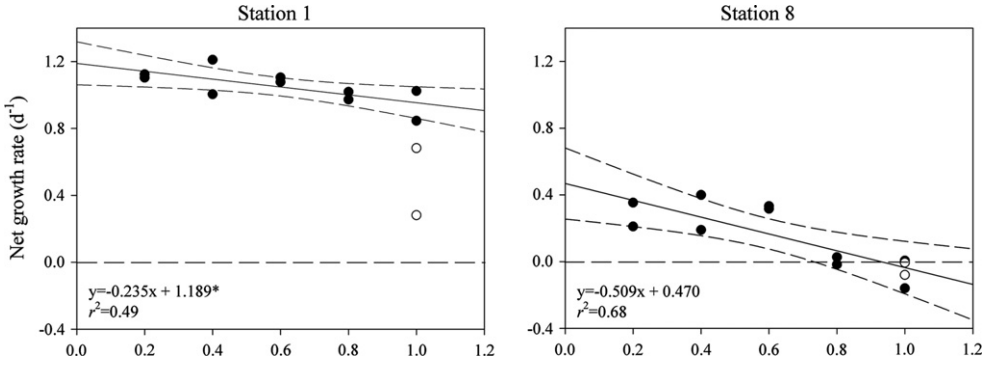

Fig. 7. Net growth rates of the aggregate Chl *a* community regressed against the whole seawater dilution factor (% whole seawater). (●) net growth rates for treatments incubated with amended nutrients. (○) net growth rates for treatments incubated without amended nutrients. Dashed lines surrounding least squares fit are 95% confidence intervals. * is the nutrient amended growth rate. Corrections to this were made (see Section 2) and the unamended growth rate is shown in Table 3.

environments (Sherr and Sherr, 1988; Calbet and Landry, 2004). This linkage is especially strong in oligotrophic regions where microbial processes dominate, and where perturbations to the equilibrium status of the physical and chemical environment are, compared to coastal environments, infrequent, thus preventing large variation in the concentration and size structure of the phytoplankton community (e.g., open subarctic Pacific Ocean). Others have reported that M_g are the dominant herbivores in the central equatorial Pacific (Landry et al., 1995a; Verity et al., 1996) and in the western edge of the ETNP (Yang et al., 2004). Less is known, however, about M_g community structure and the role of M_g in regulating surface carbon dynamics in the far eastern ETNP, where hydrographic and biological variability is comparatively more substantial than other equatorial regions (Fiedler and Talley,

Table 4
Chl *a* intrinsic growth rate (μ), and micro-grazer Chl *a*-specific grazing rate (g) from dilution experiments. Rates of primary production (PP), grazing losses (G), and % PP removed were calculated according to Landry and Calbet (2004). Numbers in parentheses are 95% confidence intervals calculated from dilution regressions. Sta: station.

Sta	Chl *a* μ (d^{-1})	Micro-grazer g (d^{-1})	PP ($\mu g\ C\ L^{-1}\ d^{-1}$)	G ($\mu g\ C\ L^{-1}$)	% PP Consumed
1	0.72 ($\pm$0.39)	0.23($\pm$0.19)	9.65	3.17	32.8
8	0.47 ($\pm$0.21)	0.51($\pm$0.32)	6.21	6.75	108.7

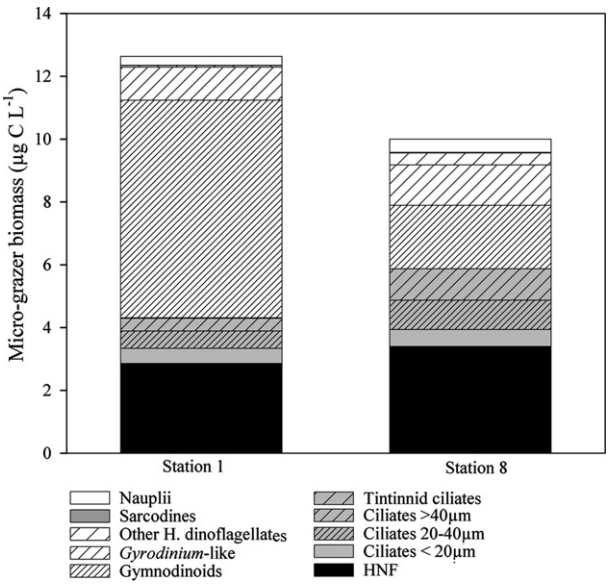

Fig. 8. Initial M_g community biomass composition from dilution grazing experiments. H: heterotrophic; HNF: heterotrophic nanoflagellates.

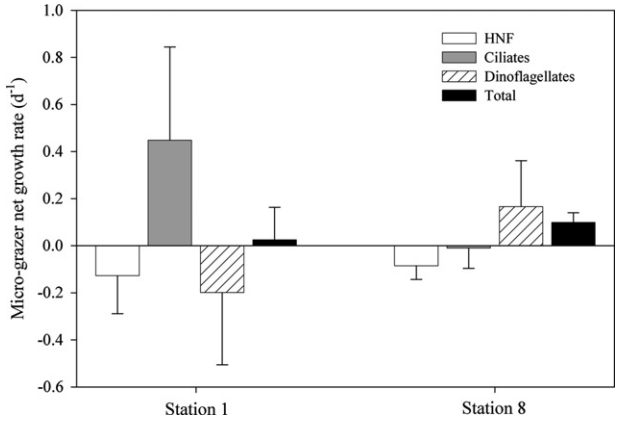

Fig. 9. Net growth rates of different M_g functional groups during 24 h grazing experiments. Net growth rates were calculated using initial 100% whole seawater and nutrient-amended 100% whole seawater dilution bottles at the end of our 24 h incubations. HNF: heterotrophic nanoflagellates.

2006; Willett et al., 2006), and where oxygen concentrations are found at limiting concentrations ($<20\ \mu mol\ kg^{-1}$) very near the surface.

The environmental and biological data collected at transect stations highlight the heterogeneity of this region. Indeed, at Stas. 4 and 5 we encountered concentrations of Chl *a* (max. Chl *a* 1.8 μg Chl *a* L^{-1}) that far exceed seasonal averages (Pennington et al., 2006). The process or processes that generated this high phytoplankton biomass remains uncertain, but based on the ETNP's well-characterized hydrography (Fiedler and Talley, 2006) and circulation (Kessler, 2006), several likely scenarios acting alone or in synergy exist. First, high surface atmospheric pressure over the Gulf of Mexico and increasing trade wind intensity beginning in the fall (Oct.) generates trans-isthmic wind jets that blow through gaps in the Sierra Madre mountain range. The wind stress curl resulting from these strong concentrated winds produce offshore-migrating eddies. These eddies generate Ekman pumping and enhanced nutrient supply to surface waters (Kessler, 2006), and are associated with elevated plankton biomass found to be transported up to 1500 km offshore (Müller-Karger and Fuentes-Yaco, 2000). Müller-Karger and Fuentes-Yaco (2000) argue that the rich chlorophyll associated with these eddies is first the product of coastal upwelling, and is later governed by upwelling within the eddy structure as it migrates offshore. These ETNP wind-jet generated eddies have been described by others (e.g., reviewed in Willett et al. (2006)) and are a principle mechanism by which nutrients and developing plankton biomass are carried offshore. Second, the Costa Rica Dome is known to vary seasonally in location, depth of thermocline shoaling, and size (Fiedler, 2002). The doming of the thermocline that we observed centered at Sta. 5 (10°41.36N, 96°20.47W) indicates that the core of the Costa Rica Dome was north and west of its average location (90°N, 90°W; Fiedler, 2002). Although this may have been the case, highest chlorophyll concentrations in the Costa Rica Dome are found from May to September, whereas during the fall months (i.e., the timing of our cruise Oct.–Nov.) high chlorophyll is typically found in the coastal boundary and migrating offshore as winter wind jets strengthen in magnitude in the fall and winter months (Fiedler, 2002). And finally, our cruise took place in the location and wake of Tropical Storm Kiko (Avila and Rhome, 2008). As such, this otherwise unproductive region (Pennington et al., 2006) was likely recently mixed and supplied with new nutrients.

Dissolved oxygen concentrations showed a doming near mid stations similar to temperature (Fig. 2). Near the center of this doming (Stas. 3–6) we observed limiting DO concentrations ($<20\ \mu mol\ kg^{-1}$) very near the surface (~25 m; Fig. 2). The very shallow OMZ, combined with high environmental and biological complexity, made an ideal setting to explore how environmental variation influences the distribution, composition, biomass, and feeding ecology of M_g in oligotrophic waters.

4.2. Micro-grazer biomass, distribution and composition

We found at the eastern edge of the ETNP that, averaged across all biochemical depth regimes, heterotrophic dinoflagellates contributed most to M_g biomass, followed by ciliates and HNF. The distribution of biomass between different M_g functional groups in this study is remarkably similar to that of other studies from the northern (Verity et al., 1996; Chavez et al., 1996; Yang et al., 2004) and southern (Masquelier and Vaulot, 2008) tropical Pacific Ocean. The closest comparison to our study is from two contrasting regimes at the western edge of the ETNP, where Yang et al. (2004) found that heterotrophic dinoflagellates dominated micro-grazer biomass (>50% of the total), followed by ciliates (20%) and HNF(16% to 21%). These independent findings showing similarity of biomass distribution between M_g functional groups across the tropical Pacific Ocean, especially the dominance of heterotrophic dinoflagellates, suggests that heterotrophic dinoflagellates play an important, if not primary, role in the consumption, remineralization, and transfer of primary production and microbially-derived organic carbon to higher trophic levels in the equatorial Pacific.

A significant finding from this research is that some of our estimates of M_g biomass at discrete depths, especially in surface

waters, are higher than have been reported in the tropical Pacific (reviewed in Yang et al., 2004). For example, Yang et al. (2004) observed micro-grazer biomass as high as 11.3 μg C L^{-1} at the western edge of the ETNP, whereas we observed M_g biomass as high as 36 μg C L^{-1} in the eastern ETNP. In an early study in the eastern tropical Pacific, high biomass (estimated as biovolume) of M_g was observed at stations near our own (Beers and Stewart, 1971). This study, however, was conducted prior to the published recognition of the microbial loop (Pomeroy, 1974; Azam et al., 1983) and of the importance of dinoflagellates as heterotrophs (Lessard and Swift, 1986); perhaps because of this, HNF and dinoflagellates were excluded from these early M_g biomass estimates. Although our data are not directly comparable, Beers and Stewart (1971) concluded that the average abundance and biovolume of M_g in the eastern tropical Pacific was comparable to, or higher than, any of their observations from coastal and oceanic locations within the California Current system (Beers and Stewart, 1967).

One explanation for our higher estimates of M_g biomass compared to other eastern tropical Pacific locations is that phytoplankton standing stock in this region is occasionally found at levels far exceeding seasonal averages (Pennington et al., 2006), and, above which, could accumulate under tight grazing regulation typical of oligotrophic ecosystems (e.g., Landry et al., 1995a, 2011; Verity et al., 1996). Instead, high phytoplankton biomass is typically produced in the coastal boundary by wind-generated upwelling, especially in the fall when high atmospheric pressure develops over the Gulf of Mexico and resultant trans-isthmic winds increase in intensity. This biomass subsequently develops and is supported by upwelling within mesoscale eddies as it is transported offshore to oligotrophic regions (Müller-Karger and Fuentes-Yaco, 2000; Willett et al., 2006). These transient events likely carry with them an associated and substantial M_g community, or support the development of one as the phytoplankton-rich water mass ages. Our highest estimate of integrated M_g biomass occurred at Sta. 5 which, based on ocean color imagery at the time of our sampling (Fig. 1), appears to have been influenced by an advected coastal water mass. Similar wind-forced eddies form in the subtropical north Pacific in the lee of the Hawaiian Islands and, like the ETNP, are regions of high plankton biomass in otherwise oligotrophic ecosystems (Brown et al., 2008). These 'intrusions' of biomass-rich water also introduce biological patchiness into the region. Indeed, our estimates of M_g biomass in waters above the pycnocline ranged from 5.6 μg C L^{-1} (well within the range of estimates from other ETP and central tropical Pacific regions) to 36.6 μg C L^{-1}. This ~6-fold difference between biomass concentrations is more variable than other regions of the tropical Pacific (Chavez et al., 1996; Yang et al., 2004).

Our measured M_g discrete depth and integrated biomass (surface to UO) correlated significantly with Chl *a* (Fig. 5). Significant correlations were also observed between M_g biomass and phytoplankton biomass at the western (Yang et al., 2004) and eastern side of the ETNP (Beers and Stewart, 1971). However, the biomass of small gymnodinoid dinoflagellates, the dominant microzooplankter in our samples, did not correlate with Chl *a*. These small (< 10 μm), green-fluorescing dinoflagellates have been observed in many marine environments (Lessard, 1991; Masquelier and Vaulot, 2008), but their feeding ecology remains poorly understood and likely includes nutritional pathways beyond direct consumption of phytoplankton. Using epifluorescent microscopy, we rarely found any of these dinoflagellates with food vacuoles containing autofluorescing autotrophic prey. On the rare occasions this was observed, the contents within the food vacuoles appeared to be the cyanobacteria, *Synecococcus*, based on presence within their food vacuoles of 1 μm to ~3 μm-sized cells with an apparent phycobiliprotein autofluorescence signature. These small dinoflagellates were the dominant M_g functional group below the UO, where Chl *a* was nearly undetectable. Podlaska et al. (2012) showed, however, substantial prokaryotic abundance and moderate heterotrophic activity and chemoautotrophic productivity below the UO, thus potentially providing these small heterotrophs with an *in situ* resource. Total biomass of ciliates positively correlated with Chl *a* biomass ($r=0.80$, $P<0.001$), suggesting that they, and not small gymnodinoid dinoflagellates, are the primary grazers of pico- and nanophytoplankton in the ETNP. Many of the observed ciliates, however, were mixotrophic and, as such, directly contributed to the standing stock of Chl *a*. This was especially true at Sta. 6, where we encountered high abundances of the near-obligate photosynthetic ciliate, *M. rubra*. Here, *M. rubra* concentrations reached over 16 μg C L^{-1} in surface waters. Ciliates are also likely imparting heavy predation pressure on HNF, as ciliate abundance was inversely correlated with the abundance of HNF (Fig. 4).

The concentration of DO did not appear to be the primary factor influencing M_g functional group composition, and perhaps to a lesser extent, M_g biomass concentration in this region of the ETNP. However, there are very few studies in pelagic marine waters exploring the species composition of M_g in relation to oxygen gradients (Zubkov et al., 1992; Fenchel et al., 1995). Of the few, it was reported that species composition of M_g changed dramatically across oxygen gradients in the Black Sea (Zubkov et al., 1992) and in Danish fjords (Fenchel et al., 1990). We did not find disparate protist communities at the interfaces of oxygen gradients, just lower biomass concentrations with depth. However, at times considerable M_g biomass was observed below the UO. For example, at Sta. 8, well within the OMZ (335 m), M_g biomass was substantial (~3 μg C L^{-1}) and the community assemblage was diverse (Table 2). These are factors we would not expect to see if DO was a limiting factor in this region.

4.3. Micro-grazer grazing and growth

Our estimated rates of phytoplankton community growth and M_g grazing varied between the two experimental stations, but for each respective measured rate, significant differences did not exist between sites. Using the average rate measurements from each site, however, shows that in the upper-mixed layer waters at our two experimental sites, grazing by the M_g community removed between 32% and >100% primary production. This range of estimates is comparable to other M_g grazing estimates from the central equatorial Pacific (Landry et al., 1995a; Verity et al., 1996) and the western ETNP (Yang et al., 2004). Using M_g biomass estimates and theoretical feeding rates, Beers and Stewart (1971) estimated that M_g grazing could consume between 39% to 104% daily phytoplankton production, nearly identical to the rates we measured. Unfortunately, time constraints prevented us from repeatedly measuring M_g grazing rates at each station and from multiple depths, thus restricting our ability to make conclusions about the daily, seasonal and depth variability in M_g grazing in this region of the ETNP.

We found that the net growth rates of the M_g community and different functional groups measured during the two dilution experiments were generally low, and sometimes negative (Fig. 8). Negative M_g net growth rates measured during dilution experiments have been reported elsewhere (Strom and Strom, 1996; Dolan et al., 2000; First et al., 2007), and the degree to which this may be an experimental artifact has been discussed (Strom et al., 2007). Because we were only able to conduct two grazing experiments we are unable to connect these findings to ETNP ecosystem processes with certitude or magnitude. Beyond the possibility of experimental artifacts causing low M_g growth rates,

other equally, if not more plausible, explanations for low M_g growth rates include low prey concentrations ($\sim$0.2 μg Chl *a* at both stations), poor prey nutritional quality (phytoplankton at Sta. 1 were nutrient limited), or intra-bottle predation. The latter may explain the negative growth rate of HNF in both experiments, as they are likely prey for both ciliates and heterotrophic dinoflagellates.

5. Conclusions

A primary finding from this research was that M_g biomass was quite high relative to estimates from other regions of the equatorial Pacific, even at locations that were oligotrophic in nature at the time of sampling. The bulk of the M_g biomass was comprised of HNF, small gymnodinoid dinoflagellates, and non-loricate oligotrich ciliates. These M_g functional groups graze primarily on bacteria, pico- and nanoeukaryotic phytoplankton. Large, diatom-consuming dinoflagellates in the genera *Gyrodinium* and *Protoperidinium* were also present in surface waters at high biomass, indicating that diatom abundance is, at times, sufficient enough to sustain a population of these large herbivores.

Biomass of M_g within the OMZ was less than we observed in surface waters, yet still substantial. The M_g functional group assemblage in these low oxygen waters was similar to those found in surface waters, suggesting that resources, rather than oxygen concentration, limit M_g biomass in the OMZ.

Acknowledgements

We thank the captain and crew of the R.V. *Seward Johnson* for their assistance at sea. Nutrient data were provided by K. Fanning (USF). This research was supported by a NSF grant OCE 0526545.

References

Avila, L.A., Rhome, J.R., 2008. The 2007 eastern Pacific hurricane season: a quiet year. Weatherwise 61 (2), 46–49.
Azam, F., Fenchel, T., Field, J.G., Gray, J.S., Meyerreil, L.A., Thingstad, F., 1983. The ecological role of water-column microbes in the sea. Mar. Ecol. Prog. Ser. 10, 257–263.
Beers, J.R., Stewart, G.L., 1967. Micro-zooplankton in the euphotic zone at five locations across the California Current. J. Fish. Res. Board Can. 24, 2053–2068.
Beers, J.R., Stewart, G.L., 1971. Micro-zooplankters in plankton communities of the upper waters of the eastern tropical Pacific. Deep Sea Res. 18 (9), 861–883.
Brown, S.L., Landry, M.R., Selph, K.E., Yang, E.J., Yoshimi, M.R., Bidigare, R.R., 2008. Diatoms in the desert: plankton community response to a mesoscale eddy in the subtropical North Pacific. Deep Sea Res. Part II 55, 1321–1333.
Calbet, A., Landry, M.R., 2004. Phytoplankton growth, microzooplankton grazing, and carbon cycling in marine systems. Limnol. Oceanogr. 49 (1), 51–57.
Chavez, F.P., 1989. Size distribution of phytoplankton in the central and eastern tropical Pacific. Global Biogeochem. Cycles 3, 27–35.
Chavez, F.P., Buck, K.R., Service, S.K., Newton, J., Barber, R.T., 1996. Phytoplankton variability in the central and eastern tropical Pacific. Deep Sea Res. Part II 43 (4–6), 835–870.
Dolan, J.R., Gallegos, C.L., Moigis, A., 2000. Dilution effects on microzooplankton in dilution grazing experiments. Mar. Ecol. Prog. Ser. 200, 127–139.
Fenchel, T., Kristensen, L.D., Rasmussen, L., 1990. Water column anoxia: vertical zonation of planktonic protozoa. Mar. Ecol. Prog. Ser. 62 (1–2), 1–10.
Fenchel, T., Bernard, C., Esteban, G., Finlay, B.J., Hansen, P.J., Iversen, N., 1995. Microbial diversity and activity in a Danish fjord with anoxic deep water. Ophelia 43, 45–100.
Fernández-Álamo, M.A., Färber-Lorda, J., 2006. Zooplankton and the oceanography of the eastern tropical Pacific: a review. Prog. Oceanogr. 69, 318–359.
Fiedler, P.C., 2002. The annual cycle and biological effects of the Costa Rica Dome. Deep Sea Res. Part I 49, 321–338.
Fiedler, P.C., Talley, L.D., 2006. Hydrography of the eastern tropical Pacific: a review. Prog. Oceanogr. 69 (2–4), 143–180.
First, M.R., Lavrentyev, P.J., Jochem, F.J., 2007. Patterns of microzooplankton growth in dilution experiments across a trophic gradient: implications for herbivory studies. Mar. Biol. 151 (5), 1929–1940.
Gordon, L.I., Jennings, Jr., J.C., Ross, A.A., Krest, J.M., 1993. A Suggested Protocol for Contiuous Flow Automated Analysis of Seawater Nutrients. WOCE Report 77 no. 68/91.
Kamykowski, D., Zentara, S.J., 1990. Hypoxia in the world ocean as recorded in the historical data set. Deep Sea Res. Part I 37 (12), 1861–1874.
Kessler, W.S., 2006. The circulation of the eastern tropical Pacific: a review. Prog. Oceanogr. 69 (2–4), 181–217.
Landry, M.R., Constantinou, J., Kirshtein, J., 1995a. Microzooplankton grazing in the central equatorial pacific during February and August, 1992. Deep Sea Res. Part II 42 (2–3), 657–671.
Landry, M.R., Kirshtein, J., Constantinou, J., 1995b. A refined dilution technique for measuring the community grazing impact of microzooplankton, with experimental tests in the central equatorial Pacific. Mar. Ecol. Prog. Ser. 120 (1–3), 53–63.
Landry, M.R., Constantinou, J., Latasa, M., Brown, S.L., Bidigare, R.R., Ondrusek, M.E., 2000. Biological response to iron fertilization in the eastern equatorial Pacific (IronEx II). III. Dynamics of phytoplankton growth and microzooplankton grazing. Mar. Ecol. Prog. Ser. 201, 57–72.
Landry, M.R., Calbet, A., 2004. Microzooplankton production in the oceans. J. Mar. Syst. 61, 501–507.
Landry, M.R., Selph, K.E., Taylor, A.G., Décima, M., Balch, W.M., Bidigare, R.R., 2011. Phytoplankton growth, grazing and production balances in the HNLC equatorial Pacific. Deep Sea Res. Part II 58 (3–4), 524–535.
Lessard, E.J., Swift, E., 1986. Dinoflagellates from the North Atlantic classified as phototrophic or heterotrophic by epifluorescence microscopy. J. Plankton Res. 8 (6), 1209–1215.
Lessard, E.J., 1991. The trophic role of heterotrophic dinoflagellates in diverse marine environments. Mar. Microb. Food Webs 5 (1), 49–58.
Masquelier, S., Vaulot, D., 2008. Distribution of micro-organisms along a transect in the South-East Pacific Ocean (BIOSOPE cruise) using epifluorescence microscopy. Biogeosciences 5, 311–321.
Menden-Deuer, S., Lessard, E.J., 2000. Carbon to volume relationships for dinoflagellates, diatoms, and other protist plankton. Limnol. Oceanogr. 45 (3), 569–579.
Müller-Karger, F.E., Fuentes-Yaco, C., 2000. Characteristics of wind-generated rings in the eastern tropical Pacific Ocean. J. Geophys. Res. 105 (C1), 1271–1284.
Parsons, T.R., Maita, Y., Lalli, C.M., 1984. A Manual of Chemical and Biological Methods for Seawater Analysis. Pergamon Press, New York, pp. 107–110.
Pennington, J.T., Mahoney, K.L., Kuwahara, V.S., Kolber, D.D., Calienes, R., Chavez, F.P., 2006. Primary production in the eastern tropical Pacific: a review. Prog. Oceanogr. 69, 285–317.
Podlaska, A., Wakeham, S.G., Fanning, K.A., Taylor, G.T., 2012. Microbial community structure and productivity in the oxygen minimum zone of the eastern tropical North Pacific. Deep Sea Res. Part I 66, 77–89.
Pomeroy, L.R., 1974. The ocean's food web, a changing paradigm. Bioscience 24 (9), 499–504.
Roff, J.C., Hopcroft, R.R., 1986. High precision microcomputer based measuring system for ecological research. Can. J. Fish. Aquat.Sci. 43, 2044–2048.
Sherr, E., Sherr, B., 1988. Role of microbes in pelagic food webs: a revised concept. Limnol. Oceanogr. 33 (5), 1225–1227.
Sherr, E.B., Sherr, B.F., 1994. Bacterivory and herbivory: key roles of phagotrophic protists in pelagic food webs. Microb. Ecol. 28 (2), 223–235.
Strom, S.L., Strom, M.W., 1996. Microplankton growth, grazing, and community structure in the northern Gulf of Mexico. Mar. Ecol. Prog. Ser. 130 (1–3), 229–240.
Strom, S.L., Macri, E.L., Olson, M.B., 2007. Microzooplankton grazing in the coastal Gulf of Alaska: variations in top-down control of phytoplankton. Limnol. Oceanogr. 52 (4), 1480–1494.
Verity, P.G., Stoecker, D.K., Sieracki, M.E., Nelson, J.R., 1996. Microzooplankton grazing of primary production at 140° W in the equatorial Pacific. Deep Sea Res. Part II 43 (4–6), 1227–1255.
Willett, C.S., Leben, R.R., Lavín, M.F., 2006. Eddies and tropical instability waves in the eastern tropical Pacific: a review. Prog. Oceanogr. 69 (2–4), 218–238.
Xie, S.P., Xu, H., Kessler, W.S., Nonaka, M., 2005. Air–sea interaction over the eastern Pacific warm pool: gap winds, thermocline dome, and atmospheric convection. J. Climate 18 (1), 5–20.
Yang, E.J., Choi, J.K., Hyun, J.H., 2004. Distribution and structure of heterotrophic protist communities in the northeast equatorial Pacific Ocean. Mar. Biol. 146 (1), 1–15.
Zubkov, M.V., Sazhin, A.F., Flint, M.V., 1992. The microplankton organisms at the oxic–anoxic interface in the pelagial of the Black Sea. FEMS Microbiol. Ecol. 101 (4), 245–250.